Cyclical variations of fluid sources and stress state in a shallow megathrust-zone mélange

Cyclical variations of fluid sources and stress state in a shallow megathrust-zone mélange

Anna Cerchiari[1], Francesca Remitti[1], Silvia Mittempergher[1,2*], Andrea Festa[3], Federico Lugli[4] and Anna Cipriani[1,5]

[1] Dipartimento di Scienze Chimiche e Geologiche, Università di Modena e Reggio Emilia, Via Campi, 103, 41125 Modena, Italy
[2] Dipartimento di Scienze dell'Ambiente e della Terra, Università di Milano Bicocca, Piazza della Scienza, 4, 20126 Milano, Italy
[3] Dipartimento di Scienze della Terra, Università di Torino, Via Valperga Caluso, 35, 10125 Torino, Italy
[4] Dipartimento di Beni Culturali, Università di Bologna, Via degli Ariani, 1, 48121 Ravenna, Italy
[5] Lamont–Doherty Earth Observatory of Columbia University, 61 Route 9W, Palisades, NY 10964-1000, USA
* Correspondence: silvia.mittempergher@unimore.it

Differences in REE patterns of calcite from extensional and shear veins of the Sestola Vidiciatico Tectonic Unit in the Northern Apennines suggest variations in fluid source during the seismic cycle in an ancient analogue of a shallow megathrust (T_{max} c. 100–150°C). In shear veins, a positive Eu anomaly suggests an exotic fluid source, probably hotter than the fault environment. Small-scale extensional veins were derived instead from a local fluid in equilibrium with the fault rocks. Mutually crosscutting relations between two extensional vein sets, parallel and perpendicular to the megathrust, suggest repeated shifting of the σ_1 and σ_3 stresses during the seismic cycle. This is consistent with: (1) a seismic phase, with brittle failure along the thrust, crystallization of shear veins from an exotic fluid, stress drop and stress rotation; (2) a post-seismic phase, with fault-normal compaction and formation of fault-normal extensional veins fed by local fluids; (3) a reloading phase, where shear stress and pore pressure are gradually restored and fault-parallel extensional veins form, until the thrust fails again. The combination of geochemical and structural analyses in veins from exhumed megathrust analogues represents a promising tool to better understand the interplay between stress state and fluids in modern subduction zones.

Subduction megathrusts have been recognized for a long time as weak interplate faults that localize deformation under low shear stresses (<20 MPa; Bird 1978; Lamb 2006; Wang and Hu 2006; Seno 2009; Duarte et al. 2015; Wang et al. 2019) and active circulation of fluids (for a review see Saffer and Tobin 2011). The weakness of megathrusts is ascribed to low-friction minerals and fluid overpressures (pore fluid factors $\lambda_V = P_f/\sigma_V > 0.9$, where P_f is the fluid pressure and σ_V is the vertical stress; Sibson 2013, and references therein), which significantly lower the effective friction coefficient of megathrust faults.

The widespread occurrence of fracture sets filled with mineral veins in fossil megathrust-related tectonic mélanges testifies to an active fluid circuit, cyclically subjected to pressure rises and drops and permeability changes related to fracturing and fracture healing by precipitation of hydrothermal minerals (e.g. Sibson 1992, 2013, 2017; Fagereng et al. 2010). Tectonic veins thus represent a valuable archive of information on both the orientations of the palaeostresses and the physicochemical characteristics of fluids circulating in the fault zone through time.

Several studies have investigated tectonic veins; for example, reconstructing stress changes and inversions during deformation history from the meso- and microstructural description of the structures (Fisher et al. 1995; Meneghini and Moore 2007; Fagereng et al. 2010; Ujiie et al. 2018), or inferring the characteristics of fluid source and circulation patterns from trace element abundances and isotope signatures retained in vein crystals (Yamaguchi et al. 2011, 2012; Lacroix et al. 2014; Dielforder et al. 2015). Structural and microstructural investigations on megathrust-related tectonic veins have led to the identification of tectonic mélanges deforming at a high angle to the maximum principal stress (e.g. Fagereng et al. 2010) or at a low angle to it (Meneghini and Moore 2007; Ujiie et al. 2018). Understanding the stress state of shallow megathrust faults is of particular interest, as it is known that large megathrust earthquakes might cause (near) complete stress drop and a switch from a compressive to a tensile stress regime in the forearc, as happened for instance after the 2011 M_W 9 Tohoku-Oki earthquake (Hasegawa et al. 2011, 2012; Ide et al. 2011; Hardebeck 2012; Lin et al. 2013; Brodsky et al. 2016, 2020).

With this work, we aim to unravel the relationships between structurally controlled fluid pathways and tectonic loading during the seismic cycle by combining petrostructural and geochemical analyses in tectonic veins sampled from an exhumed thrust surface inside the Sestola Vidiciatico Tectonic Unit in the Northern Apennines (Italy). This unit is a subduction megathrust-zone mélange representing a

field analogue for the shallow portion (T_{max} around 100–150°C) of subduction megathrusts (Vannucchi et al. 2008). We discuss the patterns of REE distribution in three types of tectonic veins and propose a reconstruction of the seismic cycle in the basal thrust of the Sestola Vidiciatico Tectonic Unit. Our findings document interrelated changes in stress state and fluid circulation, with the main seismic cycle phases involving a switching of the principal stresses, correlated with variations in fluid inputs.

Geological setting and mesoscale structure of the Vidiciatico thrust

The Sestola Vidiciatico Tectonic Unit is interpreted as a plate boundary shear zone developed in the Northern Apennines in the Early to Middle Miocene (Vannucchi et al. 2008, and reference therein), during the underthrusting of the continental Adriatic microplate below a former accretionary prism (Boccaletti et al. 1971; Coward and Dietrich 1989; Vai and Martini 2001, and reference therein). The Sestola Vidiciatico Tectonic Unit represents a complex subduction-zone mélange, which extends for about 200 km parallel to the Northern Apennines and is 200–500 m thick.

The mélange formed by the tectonic reworking and mixing of different components, including sedimentary mélanges and broken formation, derived from both the overthrusting inactive accretionary complex and its slope deposits (Remitti et al. 2007; Vannucchi et al. 2008; Festa et al. 2019). These intermixed materials are arranged in superimposing slices bounded by several thrust faults cutting through the Sestola Vidiciatico Tectonic Unit, which in turn is bounded by a basal and an upper main thrust (Vannucchi et al. 2008; Remitti et al. 2012). Vitrinite reflectance, apatite fission tracks and illite crystallinity data (Reutter 1981; Botti et al. 2004; Vannucchi et al. 2008; Thomson et al. 2010) document that the Sestola Vidiciatico Tectonic Unit experienced maximum temperatures around 120–150°C, corresponding to about 4–5 km of burial depth assuming a thermal gradient of 30°C km^{-1}.

The basal thrust, bounding the Sestola Vidiciatico Tectonic Unit from the foredeep sandstone turbidites of the underthrusting Adriatic plate (Umbria–Tuscan Units), is well exposed in the area of Vidiciatico, close to the Apennine crest (Fig. 1a; for a detailed description see Mittempergher et al. 2018), where the Sestola Vidiciatico Tectonic Unit reached its maximum burial conditions (Vannucchi et al. 2008). During its shallow depth activity, shear strain within the Vidiciatico thrust was attained in a heterogeneous shear zone, at least 1 m thick, involving mainly marls and minor clay-rich or siltstone domains (Fig. 1b–d). Deformation was partly accommodated through diffuse shearing, with multiple discontinuous fault strands contemporaneously active. At this stage, a penetrative fabric developed, consisting of rhombohedral marl lithons whose long axis is oriented at a low angle (c. 20°) to the thrust fault (Mittempergher et al. 2018). During a subsequent (mainly) brittle deformational stage, this fabric and the pre-existing diffuse deformation structures were overprinted and truncated along discrete, strain localized, shear zones (Mittempergher et al. 2018; Figs 1 and 2a). At this stage, deformation partitioned between a main fault coated by shear veins, a thin layer of strongly foliated, veined and clay-rich marls and associated minor faults, parallel or at low angle to the main fault (Fig. 1d).

Mesoscale and microscale thrust structure

The Vidiciatico thrust dips at 20° towards the WNW and is roughly parallel to the sandstone's bedding in the footwall (Figs 1a, b, d and e). The low cutoff angle to the footwall bedding suggests that the thrust had a footwall-flat geometry, and it was probably shallowly dipping when active, although its present-day attitude results from exhumation-related late tilting. Meso- and microstructural observations focus on the brittle stage of deformation of the Vidiciatico basal thrust fault (Figs 1f and 2a, b) (see detailed description by Mittempergher et al. 2018).

The thrust faults are formed by sub-millimetre scale shear surfaces coated with clay (described as microtransforms by Fagereng et al. 2010), which accommodate most of the displacement, associated with shear veins developed inside small dilational jogs. The overlapping of these shear veins up to a thickness of some centimetres gives them a striped appearance (Figs 1f and 2c) (Labaume et al. 1991; Koehn and Passchier 2000). Calcite slickenlines measured on the main and secondary faults indicate an overall top-to-the-NE sense of transport (Fig. 1c). The shear veins mostly show a crack-and-seal texture, with individual increments marked by wall-rock-inclusion trails oriented 20° ± 15° to the microtransforms (Figs 1f, 2c, d and 3a, b). The opening mode of each increment is both shear and extensional; that is, hybrid (Ramsay 1980; Ramsay and Huber 1984; Bons et al. 2012). Locally, the infill of these shear veins consists of a breccia made by fragments of the wall rock and/or pre-existent veins in a matrix of blocky calcite crystals (Figs 2b, d and 3a, c). Breccia bodies can be up to 10–20 cm thick and several decimetres long (Fig. 2b). The lack of evidence for shearing, together with their location inside dilational jogs, suggests that these veins correspond to implosion breccias (Sibson 1985, 1987), up to tens of centimetres in both thickness and length. However, the exact mechanics, kinetics and tectonic significance of this type of breccia are still unclear. Shear veins with crack-and-seal growth and with breccia infill are referred to hereafter as 'crack-and-seal shear veins' and 'breccia shear veins', respectively.

Two sets of extensional veins have been differentiated based on their orientation with respect to the main thrust fault (Fig. 2): (1) low-angle (fault-parallel) extensional veins at less than ±30° to the fault (Figs 2e, g, h and 3d, e) and (2) high-angle (fault-perpendicular) extensional veins at 70–90° to the fault (Figs 2e, g, h and 3e). Fault-parallel extensional veins are up to 1 mm thick, with a wavy, anastomosing appearance, mainly exploiting foliation surfaces or crosscutting the same foliation at low angle (Figs 2e, g, h and 3d, e) (Mittempergher et al. 2018). Calcite of these veins shows a mostly elongated blocky to fibrous texture, in many cases showing evidence for antitaxial growth (Fig. 2e and f). Fault-perpendicular extensional veins, which crosscut the fault zone at high angle (between 60 and 90°), are generally short, bounded by compositional heterogeneities (Figs 2e, g, h and 3e), and shortened along fault-parallel dissolution seams, suggesting fault-parallel flattening (Fig. 2e and g). The calcite cementing these veins is blocky to elongated blocky. Also, fault-parallel extensional veins are in many cases gently folded, and locally dislocated by microthrust faults and pressure-solution seams (Figs 2f and 3d, e), suggesting a component of fault-parallel shortening.

Fault-parallel and fault-perpendicular extensional veins mutually cut each other and are sealed by calcite with a similar orange luminescence (Supplementary material, Fig. SM1), suggesting that they were contemporaneous. Both sets of extensional veins are crosscut by shear veins (Fig. 2g), but locally shear veins are cut by extensional veins (Fig. 2g) (Mittempergher et al. 2018), suggesting that all the veins are contemporaneous and cyclically active.

At the described brittle stage, the foliation, defined by pressure-solution seams, is oriented parallel or at low angle to the thrust itself (Figs 1 and 2e, g, h). A secondary, discontinuous foliation perpendicular to the fault is visible at the microscale (Fig. 2f).

Geochemistry

Sampling and analytical methods

After detailed microstructural analyses on multiple thin sections by optical and cathodoluminescence microscope, we selected the

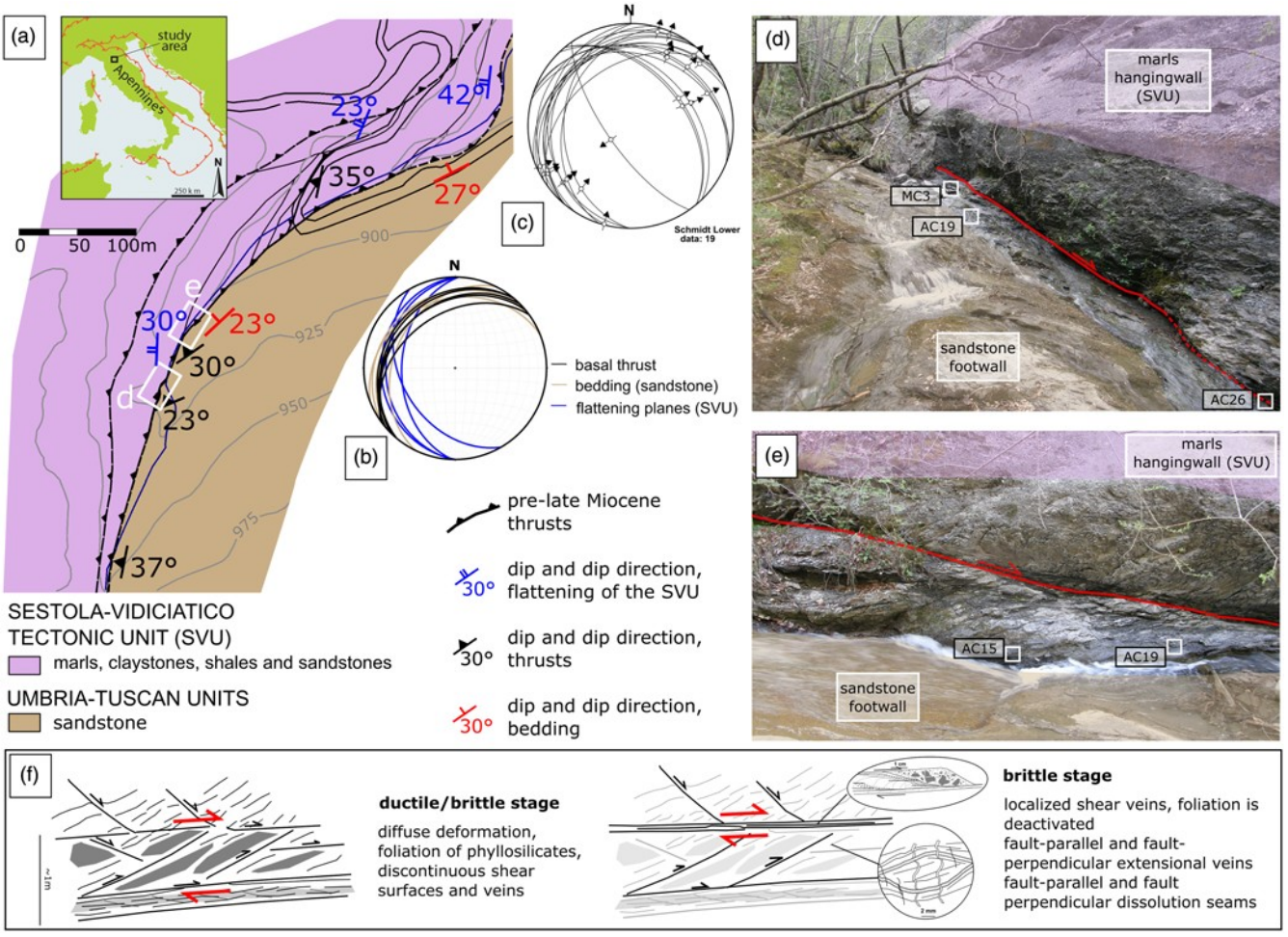

Fig. 1. Geological context of the Vidiciatico outcrop. (a) Geological map of the study area. The white rectangles highlight the locations of (d) and (e). (b) Stereoplot of the main structural elements of the Vidiciatico outcrop; namely, the bedding of the underthrusting sandstone, the main fault planes and the flattening planes within the Sestola Vidiciatico Tectonic Unit. Schmidt equal area, lower hemisphere projection. (c) Stereoplot of the shear veins and relative slip vectors, as inferred by the interpretation of calcite slickenfibres. Schmidt equal area, lower hemisphere projection. (d, e) Field photographs of the thrust, with the location of samples used for REE analysis. (f) Structural sketch and evolutionary interpretation of the meso- and microstructures of the thrust (modified after Mittempergher et al. 2018).

following samples representative of the different vein types and crosscutting veining phases (full-page thin-section scans are provided in the Supplementary material, Figs SM3–SM7).

(1) Three shear vein samples (Fig. 1d and e for location): (a) from the main thrust, cutting through the whole thrust fault zone (Mittempergher et al. 2018) (Sample AC26, Fig. 3b); (b) from a parallel smaller thrust (Sample AC15, Fig. 3a, with crack-and-seal shear veins and breccia shear veins); (c) from a decimetre-scale dilational jog along a low-angle shear fracture in the thrust fault zone (Sample MC3, breccia shear vein, Figs 2b and 3c).

(2) Three extensional vein samples (Fig. 1d and e for location): (a) 2 mm thick extensional fault-parallel veins (Sample AC3a2, Fig. 3d); (b) a < 1mm thick fault-parallel extensional vein, cut by the later MC3 breccia (Sample MC3, Fig. 3c); (c) fault-parallel and fault-perpendicular extensional veins crosscutting each other, appearing all affected by pressure-solution deformation (Sample AC19, Fig. 3e).

Major and trace elements in the veins were analysed on 100 µm thick thin sections.

In addition, five wall rock samples surrounding each selected vein (Samples AC3a2-WR, AC15-WR, AC19-WR, AC26-WR and MC3-WR) were prepared for whole-rock analyses to compare their trace element abundances with those of the respective veins.

In situ trace element analyses were determined by laser ablation inductively coupled plasma mass spectrometry (LA-ICP-MS) using a 213 nm Nd:YAG laser ablation system (NewWave Research) coupled to a quadrupole ICP-MS system (Thermo Fisher Scientific X-Series II) housed at the Centro Interdipartimentale Grandi Strumenti (CIGS) of the University of Modena and Reggio Emilia. Carbonate specimens were analysed using a laser spot size of 80 µm, a frequency of 10 Hz, a fluence of c. 6 J cm^{-2} and a He flux of 0.6 l min^{-1} (Sforna and Lugli 2017; Giovanardi et al. 2018). Prior to each analysis, the sample surface was carefully pre- ablated to remove possible contaminants. Several spot analyses were collected for each sample (Fig. 3; Supplementary materials, Figs SM3–SM7). In shear veins, points were taken parallel to the slip direction. In shear veins, particular attention was paid in selecting points as far as possible from visible wall rock inclusions. Raw ICP counts were normalized and corrected using ^{43}Ca as internal standard and NIST612 as reference material (reference mass fractions from Jochum et al. 2007, georem.mpch-mainz.gwdg.de). Relative standard deviation (RSD) was always better than 10%.

We analysed a large range of major and trace elements and used some of them to identify calcite contamination by wall-rock micro- inclusions. This was necessary because of the sampling limitations of the laser device given that during ablation it is difficult to distinguish and avoid trails of inclusions in the shear veins and wall rock clasts of the breccias (Fig. 2c and d), or partial breaching of the

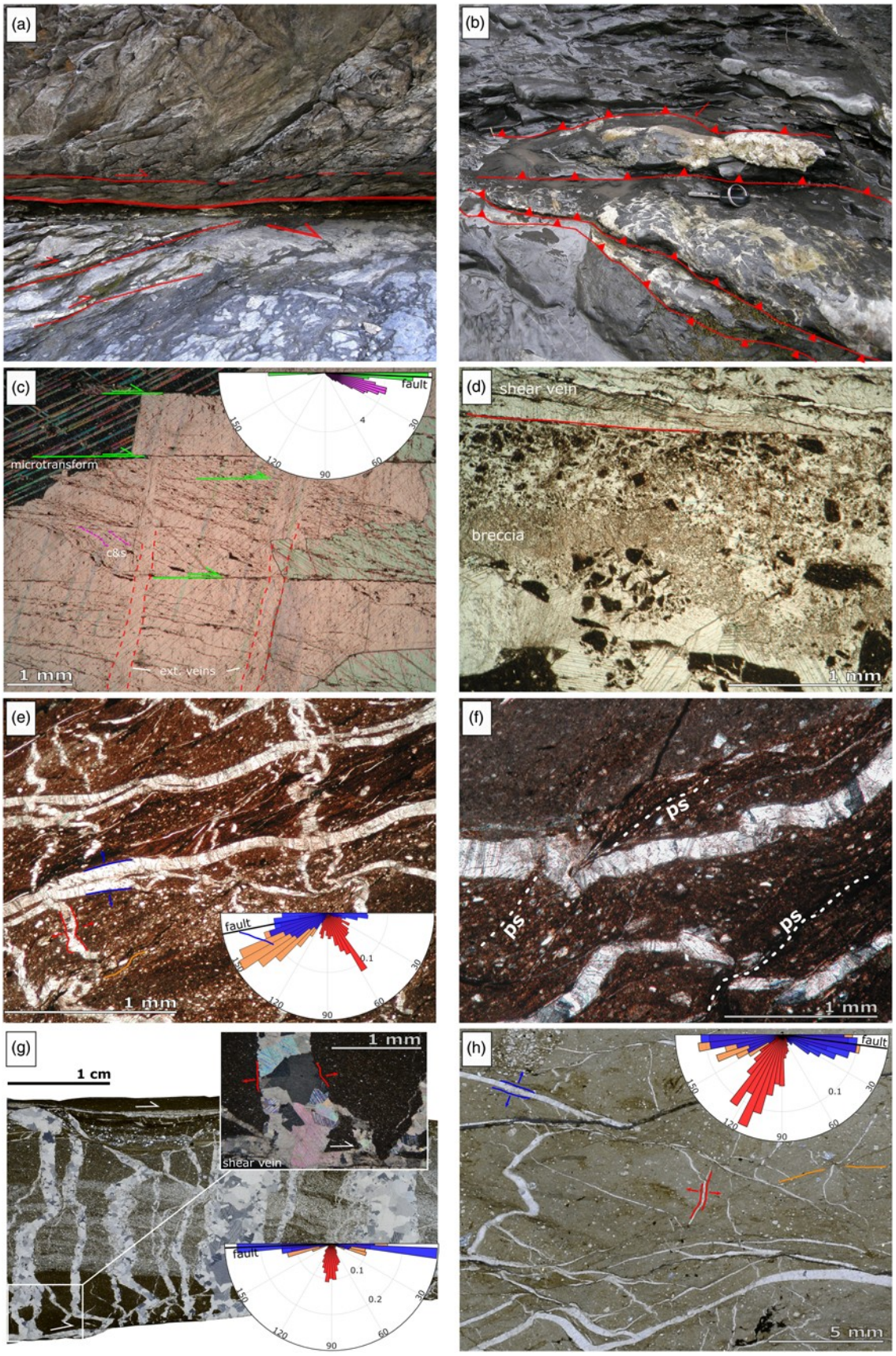

Fig. 2. Continued

wall rock of very thin extensional veins (Fig. 3e). We measured anomalously high counts of Mg, Fe, Si or K in calcites of AC26 shear vein and MC3 extensional vein and excluded these points from the dataset owing to possible wall rock contamination.

REE in wall rocks were measured in powders obtained by microdrilling of the rock samples carefully avoiding any carbonate vein. About 100 mg of powder were rinsed several times with MilliQ water, dried overnight and dissolved with a HF–HNO_3

Fig. 2. Meso- and microstructures of the Vidiciatico thrust. (a) Field photograph of the main slip surface of the thrust fault, showing the low-angle foliation defined by flattened marl lithons and some secondary shear-vein bearing fault surfaces. (b) Field picture of a dilational jog within the thrust fault zone, bounded by shear veins, where Sample MC3 was collected. (c) Detail of the internal structure of a shear vein, characterized by crack-and-seal increments lined by wall rock inclusions connected by micro-shear zones. A rose diagram shows the orientations of crack-and-seal increments (pink) and micro-shear zones (green) on the corresponding thin section. Cross-polarized light photomicrograph. (d) The texture of a breccia shear vein, with angular clasts dispersed in calcite matrix. Plane-polarized light photomicrograph. (e) Mutually crosscutting fault-perpendicular (red) and fault-parallel (blue) extensional veins. Fault- perpendicular extensional veins are shortened and folded. A rose diagram shows the orientation of pressure-solution seams (orange), and fault-parallel (blue) and fault-perpendicular (red) extensional veins with respect to the fault. (f) Detail of folded and shortened fault-parallel extensional veins, with pressure- solution seams at high angle to the fault (ps). Plane-polarized light photomicrograph. (g) Thin section scan showing mutual crosscutting relations between shear veins and fault-perpendicular extensional veins. The inset shows a detail of a fault-perpendicular extensional vein (red) crosscutting a shear vein. Cross- polarized photomicrographs. A rose diagram shows the orientation of pressure-solution seams (orange), and fault-parallel (blue) and fault-perpendicular (red) extensional veins with respect to the fault. (h) Detail of the inner part of a marl lithon crosscut by fault-parallel (blue) and fault-perpendicular (red) extensional veins. A rose diagram shows the orientation of pressure-solution seams (orange), and fault-parallel (blue) and fault-perpendicular (red) extensional veins with respect to the fault. Details of the method used for making the rose diagrams are given in the Supplementary material, Fig. SM2.

mixture. Solutions were properly diluted and analysed using a quadrupole ICP-MS X-Series II system housed at the CIGS. Data were acquired for ^{139}La, ^{140}Ce, ^{141}Pr, ^{146}Nd, ^{147}Sm, ^{153}Eu,^{157}Gd, ^{159}Tb, ^{163}Dy, ^{165}Ho, ^{166}Er, ^{169}Tm, ^{172}Yb and ^{175}Lu and calibrated using a multi-element standard solution of different concentrations (from 1 to 1000 ppb) combined with ^{115}In as an internal standard. Precisions were typically better than 5% RSD.

REE geochemistry

The chondrite-normalized REE patterns of the carbonate veins are plotted in Figure 4, according to the vein types defined by the petrostructural observations (for a complete list of REE analyses, see Supplementary material, Table SM8). Considering all the veins, the range of REE abundances is very broad, overall spanning one or two orders of magnitude, and up to one order of magnitude over a few hundred microns in a single vein. The greatest variability in REE abundances is recorded in the shear veins, whereas the smallest range is in the fault-perpendicular extensional veins.

The two samples of crack-and-seal shear veins are characterized by an Eu anomaly ranging from strongly positive to neutral and show relatively flat patterns, with variable depletion of heavy REE (HREE) and flat to strongly enriched light REE (LREE) (Fig. 4a). All AC26 patterns show a clear Eu positive anomaly, whereas in AC15 veins the positive Eu anomaly is less pronounced, or absent. The Eu anomalies are quantified, following Gao and Wedepohl (1995), as $Eu/Eu^* = Eu_N \sqrt{Sm_N \times Gd_N}$, where the subscript 'N' indicates chondrite-normalized values. Eu/Eu* values higher than 0.9 represent a positive anomaly, values lower than 0.9 a negative anomaly (Fig. 5a).

The REE patterns of the fault-parallel extensional veins (AC3a2, MC3 and AC19) can be divided into three groups (Fig. 4e). Group 1 patterns are enriched in LREE and depleted in HREE, and are present exclusively in Sample AC3a2. Group 2 patterns are convex-downward with flat HREE. Group 3 patterns are instead convex-upward, with flat LREE. Group 2 and 3 patterns are present indistinctly in Samples MC3 and AC19. Fault-perpendicular extensional veins are contained only in Sample AC19 and their REE patterns are indistinguishable from those of Group 3 fault-parallel extensional veins (Fig. 4d). Most of the breccia shear vein REE patterns resemble those of AC15 shear veins with crack-and-seal texture, but they have a variable Eu anomaly ranging from positive to slightly negative (Fig. 4b).

Wall rock REE patterns show trends consistent with those of typical sedimentary rocks, with a marked negative Eu anomaly (McLennan 1989; Plank and Langmuir 1998) (Fig. 4f). We then compare the REE composition of the wall rocks and their respective veins by normalizing the REE vein patterns to their respective wall rock REE abundances (Fig. 5b–e). Changing the normalizing factor from chondrite to wall rock scales down the overall REE abundances of the veins (Fig. 5b–e). However, the crack-and-seal shear veins maintain the positive Eu anomaly (Fig. 5b). The breccia shear veins also keep their positive or negative Eu anomaly (Fig. 5c). The extensional veins, instead, show more articulate trends of enrichment and depletion and some of their patterns acquire a small positive Eu anomaly (Fig. 5d and e).

Discussion

In this section, we first interpret the geochemical data to identify possible sources of the vein-crystallizing fluids. We then discuss the stress and fluid pressure conditions compatible with the observed structural relationships between the vein sets. Finally, we combine the geochemical and structural data to propose a model accounting for the variations in stress and fluid circulation during the seismic cycle.

Geochemistry

The REE compositions of the host rocks are within the range of comparable shaly sediments, in terms of both abundances and patterns (Fig. 4f), and in general reflect their mineral content, derived from weathering, erosion and transport of the upper continental crust. In contrast, carbonate veins show that a large variability of REE abundances occurs within the 1 m thick thrust-related shear zone, with substantial differences between vein types. The great variability in REE absolute concentrations can be linked to several factors, which include changes in REE concentration in solution, fluid oxidation state, temperature of the fluid, presence of REE-complex species and changes in flow rate (Henderson 1984). More recently, it has been argued that calcite crystallization mode, in particular crystallization rate, can also influence REE concentration in calcite (Barker et al. 2006; Barker and Cox 2011). Rapid growth of a crystal promotes the entrapment of ions concentrated in the near-surface region more effectively, whereas at a slower rate there is more time for elements in solution to diffuse through the crystal lattice and prevent the formation of a compositional zoning (Watson 2004). Therefore, the variability of the studied veins in terms of REE absolute concentration can be related to a large number of processes that cannot be individually discriminated, as also discussed by Barker and Cox (2011).

The REE patterns, whether normalized to chondrite or to the host rock itself, have some distinctive peculiarities between different vein types. Shear veins always exhibit Eu positive anomalies, whereas most extensional veins, both fault-parallel and fault-perpendicular, are characterized by negative Eu anomalies or do not present an anomaly (Fig. 5e).

The shear vein REE patterns normalized to wall rocks maintain the Eu positive anomaly, thus confirming that this feature is not related to re-equilibrium with the host rock (Fig. 4a). Positive Eu anomalies in carbonates are generated by the presence of Eu^{2+} in the fluid, as Eu^{2+} is usually taken into the calcite structure in greater proportion than any other REE^{3+}. Divalent Eu is the prevalent oxidation state for Eu in most crustal fluids at temperatures ≥200°C

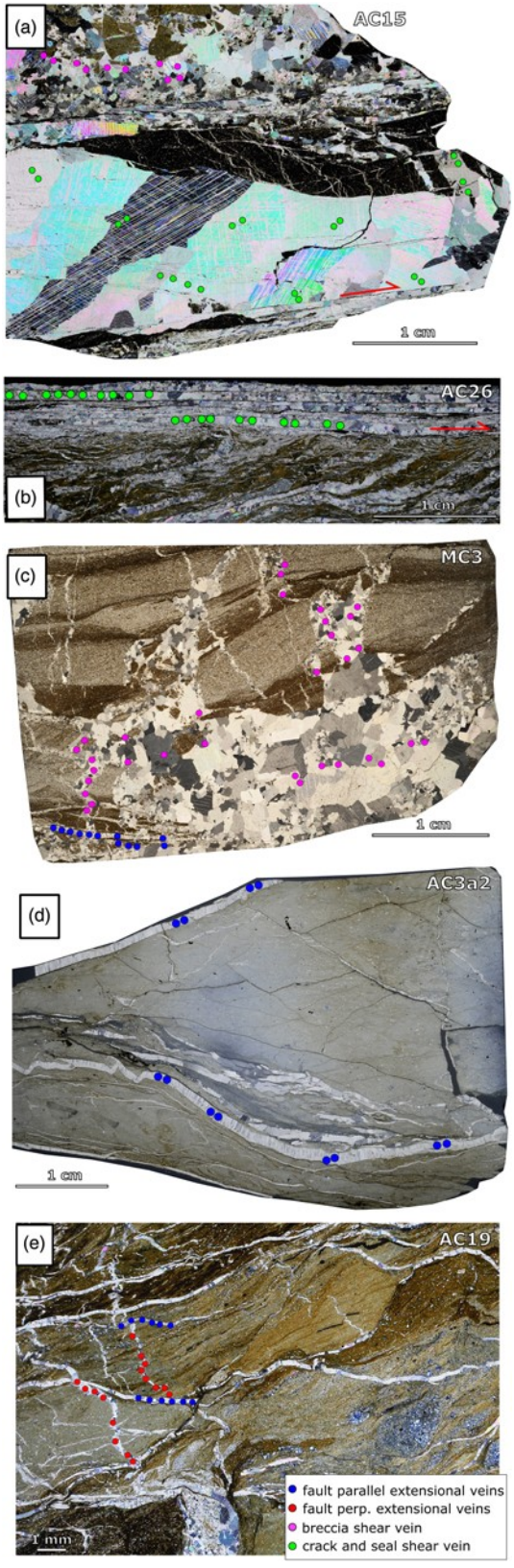

Fig. 3. Vein and wall rock samples analysed for REE content. Dots correspond to LA-ICP-MS spots. (a) Sample AC15; (b) Sample AC26; (c) Sample MC3; (d) Sample AC3a2; (e) Sample AC19. The full-page thin-section scans with labelled analysed points can be found in the Supplementary material, Figs SM3–SM7.

and in reducing environments (Bau 1991; Bau and Möller 1992). Therefore, positive Eu anomalies recorded along the basal thrust suggest that hybrid shear veins precipitated from a Eu^{2+}-enriched fluid formed in disequilibrium with the fault-zone environment, possibly at a temperature higher than the 150°C maximum of the Sestola Vidiciatico Tectonic Unit shallow portion. This is consistent with the structural localization of Vidiciatico shear veins, along thrust surfaces presumably continuous downdip for several kilometres. The larger Eu positive anomaly in AC26 veins relative to those of Sample AC15 can be caused by a larger provision of exotic fluid along the AC26 main thrust than in the AC15 minor fault. A similar disequilibrium between the shear veins and the relative wall rocks along the same fault has been previously determined by oxygen isotope analyses (Vannucchi et al. 2010).

The small negative Eu anomalies of most of the fault-parallel and fault-perpendicular extensional veins are similar to those of the wall rock samples, suggesting that calcite crystallized from a fluid in equilibrium with the thrust fault-zone environment (Fig. 4c, d and f). AC19 veins and some MC3 extensional vein patterns appear to have a small Eu positive anomaly when normalized to their respective host rock. This could reflect a small contribution of carbonate from pressure-solution of the shear veins.

LREE enrichments and HREE depletions in calcite veins are due to the different partition coefficients for the REE depending on their size (Figs 4 and 5). In fact, LREE enrichments in calcites are mostly controlled by sorption processes, where LREE are preferentially assimilated in the crystalline lattice compared with HREE (Henderson 1984; Bau 1991; Bau and Möller 1992). This process is clearly recognizable in Group 1 extensional veins, which show steep chondrite-normalized REE patterns (Fig. 4e).

Enrichments in HREE of the fluids are instead related to preferential complexing of HREE generally by CO_2-bearing fluids, which form stronger complexes with HREE than with LREE. The convex-downward patterns of calcites of Group 2 extensional veins may derive from such CO_2-bearing fluids (Fig. 4e). Some of these HREE-enriched veins are also characterized by LREE enrichments. These complex convex-upward patterns could be related to a combination of sorption and complexation processes. Veins in the Vidiciatico thrust have indeed all experienced repeated cycles of pressure-solution that might have modified their original REE content, through successive depletions of more incompatible LREE and additions of fluids derived from other dissolved veins. This is possibly best expressed by MC3 and AC19 veins (Group 2 patterns), for which we have structural evidence of pressure-solution processes (Fig. 3c and e) and which show LREE and HREE enrichments when compared with their host rock.

Breccia shear veins are very variable in terms of REE enrichments and their patterns are mostly similar to those of crack-and-seal shear veins, but the Eu anomaly varies from positive to absent (Figs 4b and 5b, e). This might indicate that fluid crystallizing breccia veins is exotic and travelling along the thrust fault, but is possibly also affected by contributions from a local source with no positive Eu anomaly. This could be related to the mechanism of implosion breccia formation (Sibson 1985): after a dilational opening along the shear surface, the pressure drop could gather the surrounding locally derived, not Eu-enriched, fluid (see for comparison Peltzer et al. 1998).

In summary, crack-and-seal shear vein patterns and Eu positive anomalies point to a source of hot fluid external to the system, which fed the incrementally growing veins repeatedly over time. Conversely, extensional vein Eu negative anomalies and variable patterns suggest that their fluid source should be internal to the system and equilibrated to the host rock, but subsequently modified by sorption and complexation reactions and pressure-solution processes. Breccia shear veins instead might have crystallized from a mixed fluid resulting from the combination of hybrid-shear-type fluids and a local source.

Differences in REE patterns between fault (along shear fractures) and extensional veins and the presence of the Eu anomaly only in the fault veins have been recorded in samples from the Mugi

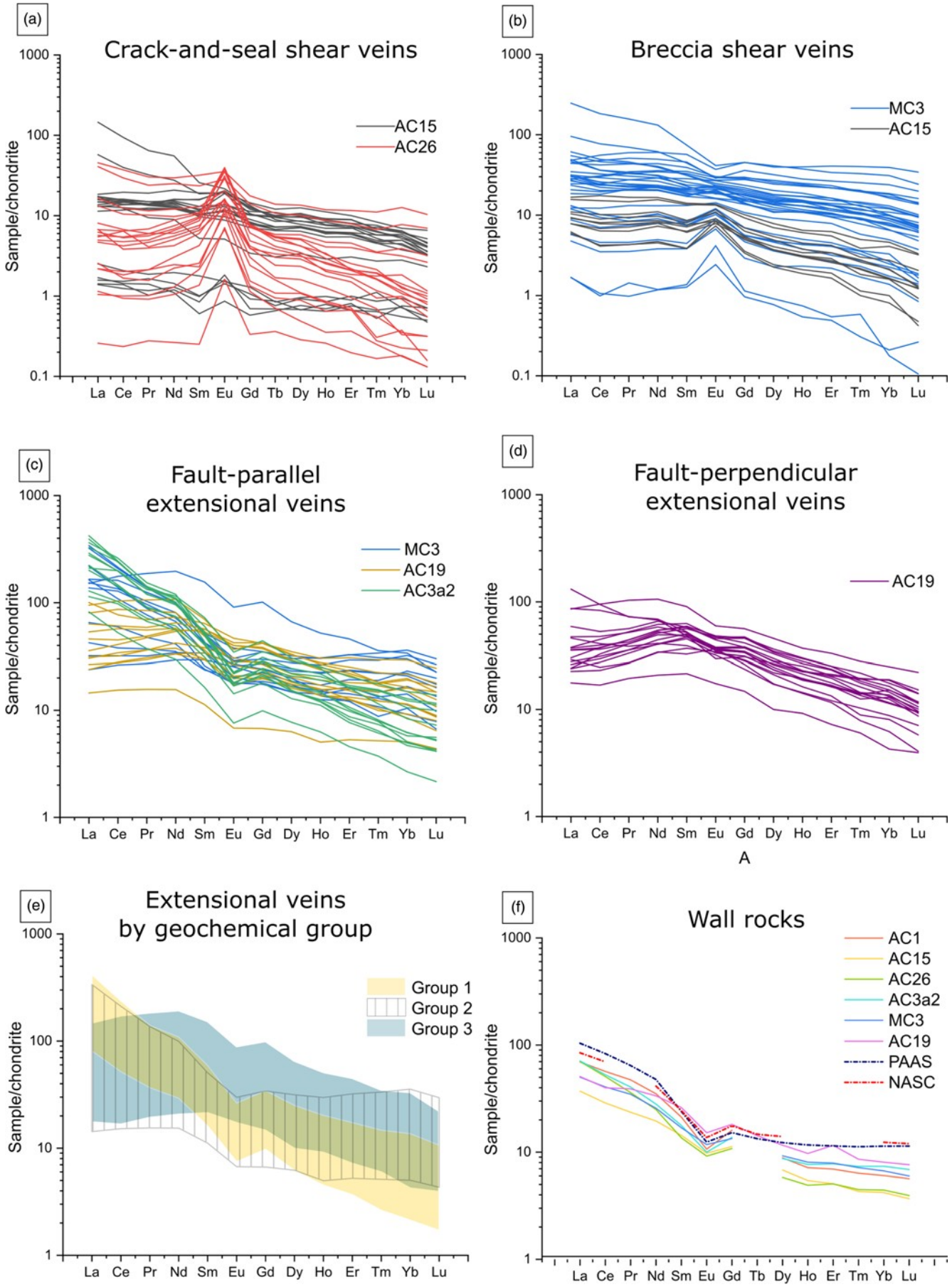

Fig. 4. REE distribution plots normalized to chondrite (Taylor and McLennan 1985): (a) crack-and-seal shear veins, separated by sample; (b) breccia shear veins, separated by sample; (c) fault-parallel extensional veins, separated by sample; (d) fault-perpendicular extensional veins in Sample AC19; (e) all extensional veins separated by groups showing similar REE patterns; (f) wall rocks, with North American Shale Composite (NASC, Gromet et al. 1984) and Post Archean Australian Shale (PAAS, Taylor and McLennan 1985) for comparison.

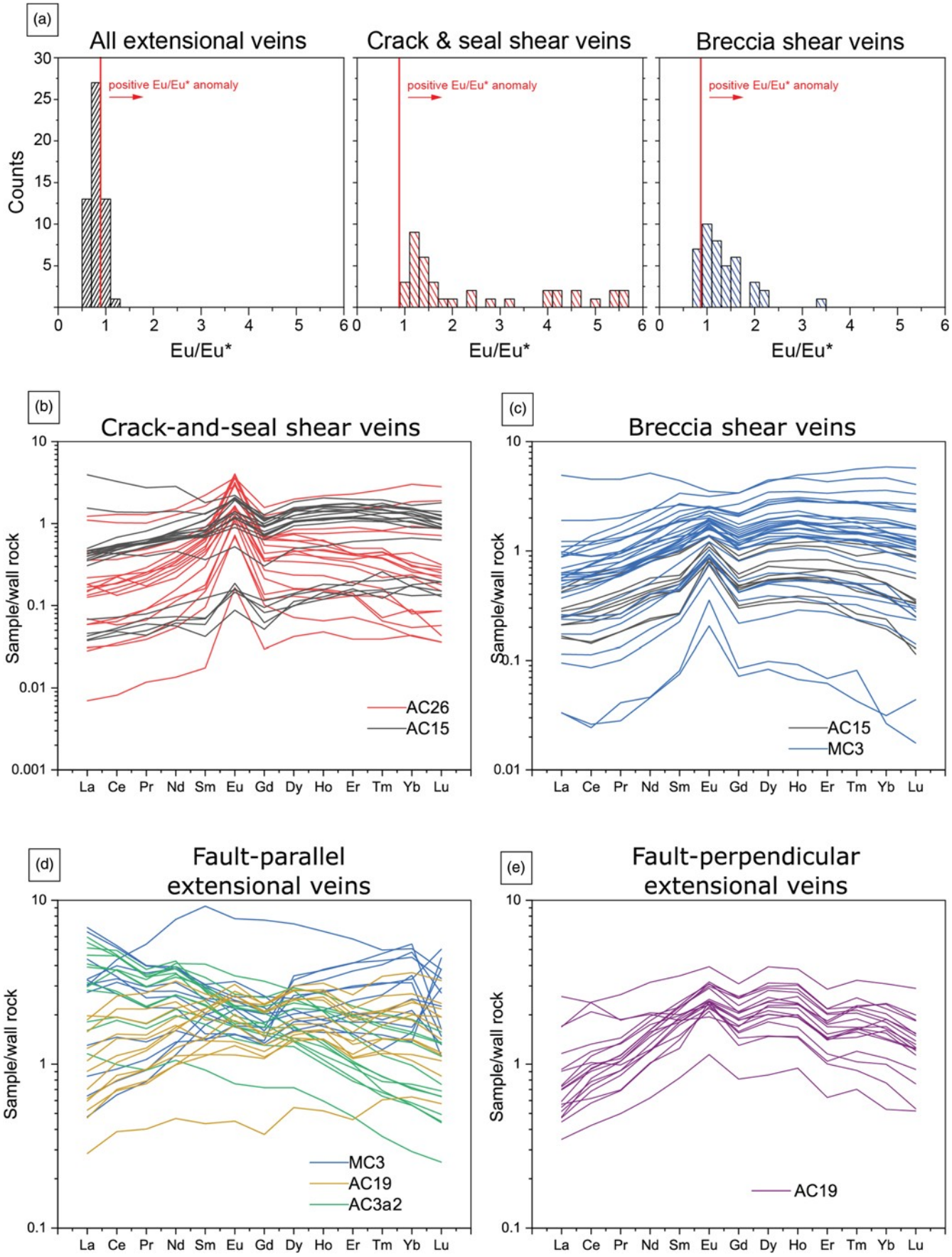

Fig. 5. Eu anomalies and REE distribution plots normalized to wall rocks. (a) Histograms of europium anomalies in extensional veins, crack-and-seal shear veins and breccia shear veins. The red line marks the value of 0.9; for higher values the Eu anomaly is positive, for lower values it is negative (Gao and Wedepohl 1995). REE distribution plots normalized to wall rocks: (b) crack-and-seal shear veins; (c) breccia shear veins; (d) fault-parallel extensional veins; (e) fault-perpendicular extensional veins in Sample AC19.

mélange in the Shimanto Belt, Japan (Yamaguchi et al. 2011). Integrating REE and C and O isotopes, Yamaguchi et al. (2011) suggested the involvement of a large-scale fluid influx, in disequilibrium with the local fluid, during the precipitation of the fault veins. Alternatively, they explained the positive Eu anomaly retained by the fault veins as due to reducing conditions developed locally along the fault plane, through production of hydrogen by co-seismic mechano-chemical reactions (Kita et al. 1982). However, a similar mechanism seems unlikely in the Vidiciatico fault zone (T_{max} <150°C), given that at low temperature the generation of a positive Eu anomaly would require an extremely low oxygen fugacity (Bau and Möller 1992).

Structural evolution of the Vidiciatico thrust

Our field and microstructural observations document mutual crosscutting relationships between different types of structural features, particularly veins, of the Vidiciatico basal thrust, that are difficult to reconcile with a single, stationary, orientation of the principal stress axes during deformation. This suggests a stress-switching between σ_1 and σ_3. In fact, the orientation of the fault-parallel extensional veins and of the discontinuous foliation, respectively at low and high angle to the main thrust fault (Fig. 2e–h), as well as the low angle between the crack-and-seal increments and the microtransforms within shear veins (Fig. 2c), are all consistent with a σ_1 oriented at low angle to the Vidiciatico basal thrust. On the contrary, fault-perpendicular extensional veins and the pressure-solution cleavage are oriented consistently with a σ_1 at high angle or perpendicular to the basal thrust (Fig. 2e, g and h). Indeed, the opening of extensional veins occurs perpendicularly to the least principal stress σ_3, by hydraulic fracturing (Secor 1965; Etheridge 1983). The orientation of the most pervasive foliation (i.e. the pressure-solution cleavage), which is subparallel to the main thrust fault and coherent with the general flattening described in the Sestola Vidiciatico Tectonic Unit at regional scale (Vannucchi et al. 2008), may reflect long-term subvertical shortening, rather than stresses driving fracturing (e.g. Fisher and Byrne 1987; Ujiie 2002; Fagereng 2013). Therefore, the documented mutual crosscutting relationships between veins and the orientation of the other, above-described, microstructures, all coherent with different orientation of the principal stress axes, might reflect a cyclical stress-switching during deformation (see also discussion by Ujiie et al. 2018). This has also been suggested for similar thrust faults around the world (e.g. Fisher and Byrne 1987; Ujiie 2002; Fagereng 2013).

To represent the stress and pore fluid pressure conditions compatible with the structural association discussed above, we use a λ–Δσ space (Sibson 1998; Cox 2010), where λ is the pore fluid factor and $\Delta\sigma = (\sigma_1 - \sigma_3)$ is the differential stress. The pore fluid factor λ is defined as $\lambda = P_f/\sigma_v$, where P_f is the pore fluid pressure and σ_v is the vertical load, here calculated for a burial depth of 5 km (Vannucchi et al. 2008) and a rock density of 2700 g cm^{-3}.

In several active megathrusts, the main principal stress reconstructed from focal mechanisms is gently (up to 30°) dipping towards the trench (Hardebeck 2015). However, as a first-order approximation, we consider a simplified model where the fault-parallel extensional veins form when $\sigma_v = \sigma_3$ and the fault-perpendicular extensional veins form when $\sigma_v = \sigma_1$ (Fig. 6a). In these circumstances, normal stress across the fault in the hanging wall (together with the mean stress) changes from greater than the vertical stress to less than the vertical stress (Sibson 2013).

Following Sibson (2013), we combined on the same λ–Δσ graph the failure and reshear envelopes for compressive ($\sigma_v = \sigma_3$) and extensional ($\sigma_v = \sigma_1$) regimes. Brittle shear failure follows the linear Coulomb criterion (blue line in Fig. 6a) $\tau = C + \mu(\sigma_n - P_f)$, where C is the cohesive strength and μ is the coefficient of internal friction, here assumed to be 0.75, a representative value for most crustal rocks (Jaeger et al. 2007). The conditions for hydraulic extensional fracturing are expressed in the form of Secor (1965) (red lines in Fig. 6a): $(\sigma_1 - \sigma_3) < 4T$ and $P_f = \sigma_3 + T$, where T is the tensional strength. The conditions for hybrid shear–extensional failure are approximated by the parabolic Griffith failure criterion (Griffith 1924) (green lines in Fig. 6a): $(\sigma_1 - \sigma_3)^2 = 8T[(\sigma_1 - P_f) + (\sigma_3 - P_f)]$. The failure envelopes were drawn in the λ–Δσ space following the recasting of Cox (2010), and adopting the widely used simplification C = 2T (Secor 1965) (Fig. 6a). Because extensional and hybrid fractures in the Vidiciatico thrust crosscut mostly marls, we use a tensional strength of 2 MPa, in the lower range for limestones or mudstone (Carmichael 1982). The conditions for opening extensional veins perpendicular to the fault zone are met in the extensional regime, with $\sigma_v = \sigma_1$, $(\sigma_v - \sigma_h) < 4T = 8$ MPa, and at suprahydrostatic to supralithostatic fluid pressures ($0.95 < \lambda < 1.015$). In contrast, extensional veins parallel to the fault form in the compressive regime, with $\sigma_v = \sigma_3$, $(\sigma_h - \sigma_v) < 4T$ and supralithostatic pore pressure (λ = 1.015). The opening of hybrid veins related to the thrust constrains the differential stress to be $4T < (\sigma_h - \sigma_v) < 5.5T$, with supralithostatic pore pressure (Fig. 6a). Hybrid-extensional fracturing along the shear veins should be contemporaneous with shear along the microtransform surfaces connecting them (Koehn and Passchier 2000; Fagereng et al. 2010), and, more generally, with shear reactivation of the thrust in the compressional field. Following the analysis of Sibson (2009, 2013) and Cox (2010), the criterion for reactivating a pre-existing fault plots as a straight line in λ–Δσ space, whose position and slope depend on fault cohesion C_f, fault friction μ_f and the reactivation angle θ_r between the fault and #σ_1. We assume a relatively low friction μ_f =0.4, coherent with shear surfaces (i.e. the microtransforms) coated by clay (mainly illite) minerals (Saffer and Marone 2003; Den Hartog et al. 2012). The widespread precipitation of calcite along the shear veins indicates that the fault was not cohesionless, but fault cohesion was probably lower than that of the wallrock, given that we observe preferential localization of successive slip episodes along the same surfaces. The dip of the thrust, and thus its reactivation angle θ_r, is poorly constrained, although probably in the range 10–20° based on the angle between microtransforms and crack-and-seal increments (Fig. 2e) and on the footwall flat geometry at the outcrop scale (Fig. 1).

Therefore, we considered the reactivation envelopes for a thrust dipping at an average angle of 15° and having cohesion between 2.5 and 3 MPa, allowing the reactivation envelope to intersect the conditions for forming hybrid fractures, as constrained by the microstructural evidence for contemporaneous slip along the microtransforms and hybrid shear–extensional fracturing (Fig. 6a). The widespread formation of extensional and hybrid fractures is another indication that cohesionless or low-cohesion thrusts are absent, otherwise they would be activated before forming extensional or hybrid fractures, for any loading path (e.g. Sibson 1998, 2013) (Fig. 6a).

A first result of this simplified analysis is that in all its brittle activity, the Vidiciatico basal thrust worked in conditions of low differential stresses (less than 11 MPa in absolute value) and high pore fluid factors (>0.95) (Fig. 6a), similar to the ambient conditions of shallow active subduction megathrusts as imaged by geophysical methods (e.g. Saffer and Tobin 2011; Hardebeck 2017). Given the very low differential stress that can be sustained by the thrust based on its mode of failure, it is reasonable that even a modest coseismic drop in shear stress would cause a long-term postseismic rotation of σ_1 (e.g. Sibson 2013). Postseismic stress rotation owing to the partial or total release of the shear stress after large megathrust earthquakes has been widely documented in active settings, where extensional faults were activated in the wedge and in the outer rise (e.g. Hasegawa et al. 2011, 2012; Ide et al. 2011; Hardebeck 2012; Brodsky et al. 2016, 2020). From the λ–Δσ diagram, it appears that

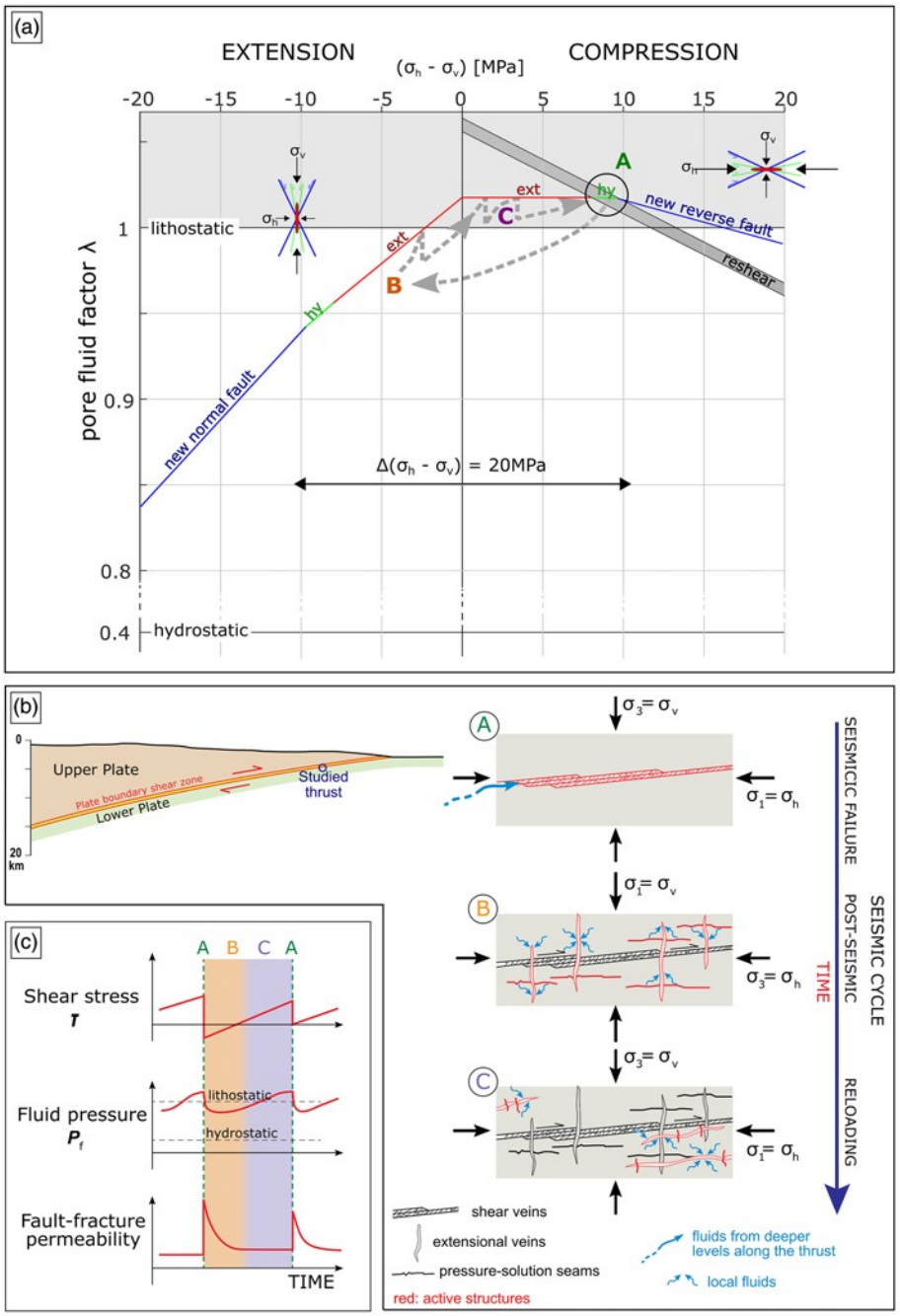

Fig. 6. Structural evolution and seismic cycle of the Vidiciatico thrust fault. (a) λ–Δσ diagram combining compressional and extensional stress regimes assuming vertical and horizontal principal stress axes, for a burial depth of 5 km. The failure envelopes for the intact wall rock and for reshear of a low-cohesion and low-angle thrust fault are drawn following the recasting of Cox (2010). A, B and C represent the stress–pore fluid conditions for reactivating the thrust together with hybrid shear extension fractures (A), forming fault-perpendicular extensional veins (B) and forming fault-parallel extensional veins (C). From the conditions A of thrust reshear, a fall in differential stress of 20 MPa (arrow) would be sufficient for a total stress reversal and formation of normal faults. (b) Interpretative sketch, with phase labels A, B and C corresponding to those in (a). During phase A, fluids from deeper levels move along the thrust, whereas in phases B and C fluid paths are local. (c) Diagram showing changes in fault strength, fluid pressure and permeability for every cycle phase (modified from Sibson 2013).

for the burial depth of the Vidiciatico thrust, a drop in differential stress of about 20 MPa (coherent with seismologically determined stress drop; Sibson 2013) can cause a complete stress switch from a compressional to an extensional regime, with the formation of optimally oriented normal faults (Fig. 6a). However, the considered dataset derives from a single outcrop and cannot be considered as representative of the whole shallow megathrust behaviour, which is probably heterogeneous. More data, hopefully from different fossil analogues, are necessary to drive more robust conclusions at a larger scale.

Stress–fluid interplay during the seismic cycle

The geochemical signatures of the vein sets in the Vidiciatico thrust are strongly correlated with their structural significance. Shear veins, associated with shear failure along the thrust, bear evidence for the influx of fluids external to the system, whereas small-scale extensional veins are cemented by local fluids in equilibrium with the surrounding rocks, independently of their orientation. Brittle failure mode appears thus to be strongly coupled with fluid transport, as expected for low- porosity rocks such as the tectonized marls hosting the Vidiciatico thrust fault (e.g. Cox 2010; Sibson 2013). Based on the above analysis of the differential stress–pore fluid pressure conditions necessary to form the vein sets and their mutually crosscutting relationships, we propose a model in which the activity of the basal thrust occurred through the following cyclically repeated phases.

(1) Seismic failure along the thrust. The differential stress–pore fluid factor conditions are within the area A in Figure 6a, meeting both the conditions for reshear on the main fault and those for opening of shear veins inside small dilational jogs. The earthquake ruptures, which probably nucleated in deeper sectors of the fault, can cause a drop in differential stress sufficient to switch the stress state of the area from a subvertical σ_3 to a subvertical σ_1. This differential stress fall is associated with a drop in pore fluid pressure caused mainly by two factors: the poroelastic relaxation owing to

the drop in mean stress, expressed by the Skempton coefficient (e.g. Sibson 2013), and the increase in fracture permeability caused by the coseismic damage (e.g. Sibson 1986; Mitchell and Faulkner 2012). Coseismic fluid drainage is in agreement with the positive Eu* anomaly of crack-and-seal shear veins and, to a lesser extent, of implosion breccias, which points to fluids sourced by deeper reservoirs in disequilibrium with the thrust wall rock (Fig. 6b and c).
(2) Postseismic phase. After the earthquake, as a result of the simultaneous drop in both differential stress and pore pressure, the conditions of the faults in λ–Δσ space are within the area B in Figure 6a. The fault then undergoes compaction, which causes a reduction of porosity and consequent pore fluid pressure increase (e.g. Sleep and Blanpied 1992). An increase in pore fluid pressure can lead to the onset of extensional failure in the extensional regime, thus producing fault-perpendicular extensional veins (B in Fig. 6a and b). The pore pressure excesses are likely to be local and immediately discharged by the formation of the veins, thus limiting the increase in pore fluid pressure. The REE patterns of fault-perpendicular extensional veins are buffered by the wall rock, as expected for small fractures draining local fluids. Gradually, as fault strength recovers, tectonic loading causes a gradual increase in σ_h and a reduction in $(\sigma_v - \sigma_h)$, and the stress state moves towards C (arrow in Fig. 6a).

(3) Reloading phase. The increase in σ_h owing to tectonic loading allows the differential stress to decrease in absolute value, and subsequently to switch to a compressional regime, with pore fluid pressure limited by the formation of subhorizontal extensional veins (C in Fig. 6a and b). Accordingly, subhorizontal extensional veins precipitate calcite from local fluids, in equilibrium with the wall rock (REE patterns buffered by the host rocks) and affected by pressure-solution, owing to fault-parallel shortening. Strength, pore fluid and stress recover in the compressional regime (Fig. 6b). The formation of extensional veins excludes the contemporaneous presence of a well-oriented cohesionless fault (e.g. Sibson 1998, 2013). Therefore, at this stage the thrust has regained some cohesion probably through calcite precipitation.

(4) Back to phase (1). The increase in σ_h owing to tectonic loading causes an increase in differential stress leading to the reactivation of the thrust (A in Fig. 6).

Concluding remarks

We analysed the petrostructure and geochemical composition of tectonic veins sampled from an exhumed thrust surface inside the Sestola Vidiciatico Tectonic Unit fault zone (Northern Apennines, Italy), which represents a field analogue for the shallow portion (T_{max} around 100–150°C) of subduction megathrusts (Vannucchi et al. 2008). The combination of REE composition and structural data suggests the following.

(1) The stress along the fault cyclically switched from a compressional reverse-slip faulting pre- to syn-failure (σ_1 at low angle to the fault), to extensional normal-slip faulting post-failure (σ_1 at high angle to the fault).
(2) This switching is compatible with a complete release of the shear stress along the thrust fault surface, as observed in modern subduction zones (e.g. Lin et al. 2013; Brodsky et al. 2016).

(3) The complete release of shear stress is coherent with a low differential stress before the event, as constrained by the formation of vein sets during and before the event.

(4) Thrust activity is correlated with changes in permeability, with inputs into the system of an external fluid marked by an Eu positive anomaly, during the main seismic event, and a local fluid source, with no Eu anomaly, in the post-seismic and reloading phases. A similar interpretation has been given by Yamaguchi et al. (2011) to explain the REE signatures of quartz–calcite veins of the Mugi mélange in the Shimanto Belt, Japan, which have REE patterns and Eu anomalies very similar to those of the Vidiciatico shear veins.

To conclude, our results indicate that the combination of geochemical and structural analyses on veins from megathrust field analogues represents a promising tool towards a deeper understanding of the interplay between stress state and fluids in subduction zones. In particular, the oxidation–reduction behaviour of Eu is central to identify the redox ambient conditions and trace possible inputs of external fluids. It remains to be seen whether the high variability of the REE patterns, which characterize the Vidiciatico veins, will be confirmed in other similar tectonic settings. Moreover, our data support that the seismic cycle is closely dependent on both the reaccumulation of fluid overpressure along the plate interface and the accumulation of shear–strain along the megathrust, as proposed by Sibson (2013) for the 2011 M_S 9.0 Tohoku-Oki megathrust rupture.

Acknowledgements We thank two anonymous reviewers and N. J. Phillips for their constructive and inspiring comments, which helped us to significantly improve our paper.

References

Barker, S.L.L. and Cox, S.F. 2011. Oscillatory zoning and trace element incorporation in hydrothermal minerals: insights from calcite growth experiments. Geofluids, 11, 48–56, https://doi.org/10.1111/j.1468-8123.2010.00305.x

Barker, S.L.L., Cox, S.F., Eggins, S.M. and Gagan, M.K. 2006. Microchemical evidence for episodic growth of antitaxial veins during fracture-controlled fluid flow. Earth and Planetary Science Letters, 250, 331–344, https://doi.org/10.1016/j.epsl.2006.07.051

Bau, M. 1991. Rare-earth element mobility during hydrothermal and metamorphic fluid–rock interaction and the significance of the oxidation state of europium. Chemical Geology, 93, 219–230, https://doi.org/10.1016/0009-2541(91)90115-8

Bau, M. and Möller, P. 1992. Rare earth element fractionation in metamorphogenic hydrothermal calcite, magnesite and siderite. Mineralogy and Petrology, 45, 231–246, https://doi.org/10.1007/BF01163114

Bird, P. 1978 Initiation of intracontinental subduction in the Himalaya. Journal of Geophysical Research: Solid Earth, 83, 4975–4987, https://doi.org/10.1029/JB083iB10p04975

Boccaletti, M., Elter, P. and Guazzone, G. 1971. Plate tectonic models for the development of the Western Alps and Northern Apennines. Nature Physical Science, 234, 108–111, https://doi.org/10.1038/physci234108a0

Bons, P.D., Elburg, M.A. and Gomez-Rivas, E. 2012. A review of the formation of tectonic veins and their microstructures. Journal of Structural Geology, 43, 33–62, https://doi.org/10.1016/j.jsg.2012.07.005

Botti, F., Aldega, L. and Corrado, S. 2004. Sedimentary and tectonic burial evolution of the Northern Apennines in the Modena–Bologna area: constraints from combined stratigraphic, structural, organic matter and clay mineral data of Neogene thrust-top basins. Geodinamica Acta, 17, 185–203, https://doi.org/10.3166/ga.17.185-203

Brodsky, E.E., Saffer, D., Fulton, P., Chester, F., Conin, M., Huffman, K. and Moore, J.C. 2016. The postearthquake stress state on the Tohoku megathrust as constrained by reanalysis of the JFAST breakout data. Geophysical Research Letters, 44, 8294–8302, https://doi.org/10.1002/2017GL074027

Brodsky, E.E., Mori, J.J. et al. 2020. The state of stress on the fault before, during, and after a major earthquake. Annual Review of Earth and Planetary Sciences, 48, https://doi.org/10.1146/annurev-earth-053018-060507

Carmichael, R.S. 1982. Handbook of Physical Properties of Rocks, 2. CRC Press, Boca Raton, FL.

Coward, M. and Dietrich, D. 1989. Alpine tectonics – an overview. Geological Society, London, Special Publications, 45, 1–29, https://doi.org/10.1144/GSL.SP.1989.045.01.01

Cox, S.F. 2010. The application of failure mode diagrams for exploring the roles of fluid pressure and stress states in controlling styles of fracture-controlled permeability enhancement in faults and shear zones. Geofluids, 10, 217–233, https://doi.org/10.1111/j.1468-8123.2010.00281.x

den Hartog, S.A.M., Peach, C., de Winter, D.A.M., Spiers, C.J. and Shimamoto, T. 2012. Frictional properties of megathrust fault gauges at low sliding velocities: New data on effects of normal stress and temperature. Journal of Structural Geology, 38, 156–171, https://doi.org/10.1016/j.jsg.2011.12.001

Dielforder, A., Vollstaedt, H., Vennemann, T., Berger, A. and Herwegh, M. 2015. Linking megathrust earthquakes to brittle deformation in a fossil accretionary complex. Nature Communications, 6, https://doi.org/10.1038/ncomms8504

Duarte, J.C., Schellart, W.P. and Cruden, A.R. 2015. How weak is the subduction zone interface? Geophysical Research Letters, 42, 2664–2673, https://doi.org/10.1002/2014GL062876

Etheridge, M.A. 1983. Differential stress magnitudes during regional deformation and metamorphism: upper bound imposed by tensile fracturing. Geology 11, 231–234. https://doi.org/10.1130/0091-7613(1983)11<231:DSMDRD>2.0.CO;2

Fagereng, Å. 2013. On stress and strain in a continuous–discontinuous shear zone undergoing simple shear and volume loss. Journal of Structural Geology, 50, 44–53, https://doi.org/10.1016/j.jsg.2012.02.016

Fagereng, Å, Remitti, F. and Sibson, R.H. 2010. Shear veins observed within anisotropic fabric at high angles to the maximum compressive stress. Nature Geoscience, 3, 482–485, https://doi.org/10.1038/ngeo898

Festa, A., Pini, G.A., Ogata, K. and Dilek, Y. 2019. Diagnostic features and field criteria in recognition of tectonic, sedimentary and diapiric mélanges in orogenic belts and exhumed subduction–accretion complexes. Gondwana Research, 74, 7–30, https://doi.org/10.1016/j.gr.2019.01.003

Fisher, D.M. and Byrne, T. 1987. Structural evolution of underthrusted sediments, Kodiak Islands, Alaska. Tectonics, 6, 775–793, https://doi.org/10.1029/TC006i006p00775

Fisher, D.M., Brantley, S.L., Everett, M. and Dzvonik, J. 1995. Cyclic fluid flow through a regionally extensive fracture network within the Kodiak accretionary prism. Journal of Geophysical Research, 100, 12881–12894, https://doi.org/10.1029/94JB02816

Gao, S. and Wedepohl, K.H. 1995. The negative Eu anomaly in Archean sedimentary rocks: Implications for decomposition, age and importance of their granitic sources. Earth and Planetary Science Letters, 133, 81–94, https://doi.org/10.1016/0012-821X(95)00077-P

Giovanardi, T., Mazzucchelli, M., Lugli, F., Girardi, V.A., Correia, C.T., Tassinari, C.C. and Cipriani, A. 2018. Isotopic constraints on contamination processes in the Tonian Goiás Stratiform Complex. Lithos, 310, 136–152, https://doi.org/10.1016/j.lithos.2018.04.008

Griffith, A. A. 1924. The theory of rupture. Proceedings of 1st International Congress on Applied Mechanics, Delft, 55–63.

Gromet, L.P., Dymek, R.F., Haskin, L.A. and Korotev, R.L. 1984. The "North American shale composite": Its compilation, major and trace element characteristics. Geochimica et Cosmochimica Acta, 48, 2469–2482, https://doi.org/10.1016/0016-7037(84)90298-9

Hardebeck, J.L. 2012. Coseismic and postseismic stress rotations due to great subduction zone earthquakes. Geophysical Research Letters, 39, L21313, https://doi.org/10.1029/2012GL053438

Hardebeck, J.L. 2015. Stress orientations in subduction zones and the strength of subduction megathrust faults. Science, 349, 1213–1216, https://doi.org/10.1126/science.aac5625

Hardebeck, J.L. 2017. The spatial distribution of earthquake stress rotations following large subduction zone earthquakes. Earth, Planets and Space, 69, 69, https://doi.org/10.1186/s40623-017-0654-y

Hasegawa, A., Yoshida, K. and Okada, T. 2011. Nearly complete stress drop in the 2011 M_w 9.0 off the Pacific coast of Tohoku Earthquake. Earth, Planets and Space, 63, 703–707, https://doi.org/10.5047/eps.2011.06.007

Hasegawa, A., Yoshida, K., Asano, Y., Okada, T., Iinuma, T. and Ito, Y. 2012. Change in stress field after the 2011 great Tohoku-Oki earthquake. Earth and Planetary Science Letters, 355–356, 231–243, https://doi.org/10.1016/j.epsl.2012.08.042

Henderson, P. 1984. Rare Earth Element Geochemistry. Developments in Geochemistry, Vol. 2. Elsevier, Oxford.

Ide, S., Baltay, A. and Beroza, G.C. 2011. Shallow dynamic overshoot and energetic deep rupture in the 2011 Mw 9.0 Tohoku-Oki earthquake. Science, 332, 1426–1429, https://doi.org/10.1126/science.1207020

Jaeger, J.C., Cook, N.G.W. and Zimmerman, R.W. 2007. Fundamental of Rock Mechanics. Fourth Edition, Blackwell Publishing.

Jochum, K.P., Hofmann, A.W., Herwig, K., Lammel, E., Stoll, B. and Nohl, U. 2007. GeoReM: A New Geochemical Database for Reference Materials and Isotopic Standards. Geostandards and Geoanalytical Research, 29, 333–338, https://doi.org/10.1111/j.1751-908X.2005.tb00904.x

Kita, I., Matsuo, S. and Wakita, H. 1982. H_2 generation by reaction between H_2O and crushed rock: an experimental study on H_2 degassing from the active fault zone. Journal of Geophysical Research, 87, https://doi.org/10.1029/JB087iB13p10789

Koehn, D. and Passchier, C.W. 2000. Shear sense indicators in striped bedding-veins. Journal of Structural Geology, 22, 1141–1151, https://doi.org/10.1016/S0191-8141(00)00028-6

Labaume, P., Berty, C. and Laurent, P.H. 1991. Syn-diagenetic evolution of shear structures in superficial nappes: an example from the Northern Apennines. Journal of Structural Geology, 13, 385–398, https://doi.org/10.1016/0191-8141(91)90012-8

Lacroix, B., Travé, A., Buatier, M., Labaume, P., Vennemann, T. and Dubois, M. 2014. Syntectonic fluid-flow along thrust faults: Example of the South-Pyrenean fold-and-thrust belt. Marine and Petroleum Geology, 49, 84–98, https://doi.org/10.1016/j.marpetgeo.2013.09.005

Lamb, S. 2006. Shear stresses on megathrusts: Implications for mountain building behind subduction zones. Journal of Geophysical Research, 111, B07401, https://doi.org/10.1029/2005JB003916

Lin, W., Conin, M. et al. 2013. Stress state in the largest displacement area of the 2011 Tohoku-Oki earthquake. Science, 339, 687–690, https://doi.org/10.1126/science.1229379

McLennan, S.M. 1989. Rare earth elements in sedimentary rocks: influence of provenance and sedimentary process. Mineralogical Society of America, Reviews in Mineralogy, 21, 169–200.

Meneghini, F. and Moore, J.C. 2007. Deformation and hydrofracture in a subduction thrust at seismogenic depths: The Rodeo Cove thrust zone, Marin Headlands, California. Geological Society of America Bulletin, 119, 174–183, https://doi.org/10.1130/B25807.1

Mitchell, T.M. and Faulkner, D.M. 2012. Towards quantifying the matrix permeability of fault damage zones in low porosity rocks. Earth and Planetary Science Letters, 339, 24–31, https://doi.org/10.1016/j.epsl.2012.05.014

Mittempergher, S., Cerchiari, A., Remitti, F. and Festa, A. 2018. From soft sediment deformation to fluid assisted faulting in the shallow part of a subduction megathrust analogue: the Sestola Vidiciatico tectonic Unit (Northern Apennines, Italy). Geological Magazine, 155, 438–450, https://doi.org/10.1017/S0016756817000668

Peltzer, G., Rosen, P., Rogez, F. and Hudnut, K. 1998. Poroelastic rebound along the Landers 1992 earthquake surface rupture. Journal of Geophysical Research: Solid Earth, 103, 30131–30145, https://doi.org/10.1029/98JB02302

Plank, T. and Langmuir, C.H. 1998. The chemical composition of subducting sediment and its consequences for the crust and mantle. Chemical Geology, 145, 325–394, https://doi.org/10.1016/S0009-2541(97)00150-2

Ramsay, J.G. 1980. Shear zone geometry: a review. Journal of Structural Geology, 2, 83–89, https://doi.org/10.1016/0191-8141(80)90038-3

Ramsay, J.G. and Huber, M.I. 1984. The Techniques of Modern Structural Geology, Vol. 1: Strain Analysis. Academic Press, London.

Remitti, F., Bettelli, G. and Vannucchi, P. 2007. Internal structure and tectonic evolution of an underthrust tectonic melange: the Sestola–Vidiciatico tectonic unit of the Northern Apennines, Italy. Geodinamica Acta, 20, 37–51, https://doi.org/10.3166/ga.20.37-51

Remitti, F., Bettelli, G., Panini, F., Carlini, M. and Vannucchi, P. 2012. Deformation, fluid flow, and mass transfer in the forearc of convergent margins: A two-day field trip in an ancient and exhumed erosive convergent margin in the Northern Apennines. GSA Field Guides, 28, 1–33, https://doi.org/10.1130/2012.0028(01)

Reutter, K.J. 1981. A trench–forearc model for the Northern Apennines. In: Wezel, F.C. (ed.) Sedimentary Basins of Mediterranean Margins. Tecnoprint, Bologna, 435–443.

Saffer, D.M. and Marone, C. 2003. Comparison of smectite- and illite-rich gouge frictional properties: application to the updip limit of the seismogenic zone along subduction megathrusts. Earth and Planetary Science Letters, 215, 219–235, https://doi.org/10.1016/S0012-821X(03)00424-2

Saffer, D.M. and Tobin, H.J. 2011. Hydrogeology and mechanics of subduction zone forearcs: fluid flow and pore pressure. Annual Review of Earth and Planetary Sciences, 39, 157–186, https://doi.org/10.1146/annurev-earth-040610-133408

Secor, D.T. 1965. Role of fluid pressure in jointing. American Journal of Science, 263, 633–646, https://doi.org/10.2475/ajs.263.8.633

Seno, T. 2009. Determination of the pore fluid pressure ratio at seismogenic megathrusts in subduction zones: Implications for strength of asperities and Andean-type mountain building. Journal of Geophysical Research, 114, B05405, https://doi.org/10.1029/2008JB005889

Sforna, M.C. and Lugli, F. 2017. MapIT!: a simple and user-friendly MATLAB script to elaborate elemental distribution images from LA-ICP-MS data. Journal of Analytical Atomic Spectrometry, 32, 1035–1043, https://doi.org/10.1039/C7JA00023E

Sibson, R.H. 1985. Stopping of earthquake ruptures at dilatational jogs. Nature, 316, 248–251, https://doi.org/10.1038/316248a0

Sibson, R.H. 1986. Brecciation processes in fault zones: Inferences from earthquake rupturing. Pure and Applied Geophysics, 124, 159–175, https://doi.org/10.1007/BF00875724

Sibson, R.H. 1987. Earthquake rupturing as a mineralizing agent in hydrothermal systems. Geology, 15, 701–704, https://doi.org/10.1130/0091-7613(1987)15<701:ERAAMA>2.0.CO;2

Sibson, R.H. 1992. Implications of fault-valve behaviour for rupture nucleation and recurrence. Tectonophysics, 211, 283–293, https://doi.org/10.1016/0040-1951(92)90065-E

Sibson, R.H. 1998. Conditions for fault-valve behaviour. Geological Society, London, Special Publications, 54, 15–28, https://doi.org/10.1144/GSL.SP.1990.054.01.02

Sibson, R.H. 2009. Rupturing in overpressured crust during compressional inversion – the case from NE Honshu, Japan. Tectonophysics, 473, 404–416, https://doi.org/10.1016/j.tecto.2009.03.016

Sibson, R.H. 2013. Stress switching in subduction forearcs: Implications for overpressure containment and strength cycling on megathrusts. Tectonophysics, 600, 142–152, https://doi.org/10.1016/j.tecto.2013.02.035

Sibson, R.H. 2017. Tensile overpressure compartments on low-angle thrust faults. Earth, Planets and Space, 69, 1–15, https://doi.org/10.1186/s40623-017-0699-y

Sleep, N.H. and Blanpied, M.L. 1992. Creep, compaction and the weak rheology of major faults. Nature, 359, 687, https://doi.org/10.1038/359687a0

Taylor, S.R. and McLennan, S.M. 1985. The Continental Crust: Its Composition and Evolution. Blackwell, Oxford.

Thomson, S.N., Brandon, M.T., Reiners, P.W., Zattin, M., Isaacson, P.J. and Balestrieri, M.L. 2010. Thermochronologic evidence for orogen-parallel variability in wedge kinematics during extending convergent orogenesis of the northern Apennines, Italy. Geological Society of America Bulletin, 122, 1160–1179, https://doi.org/10.1130/B26573.1

Ujiie, K. 2002. Evolution and kinematics of an ancient décollement zone, mélange in the Shimanto accretionary complex of Okinawa Island, Ryukyu Arc. Journal of Structural Geology, 24, 937–952, https://doi.org/10.1016/S0191-8141(01)00103-1

Ujiie, K., Saishu, H., Fagereng, Å, Nishiyama, N., Otsubo, M., Masuyama, H. and Kagi, H. 2018. An explanation of episodic tremor and slow slip constrained by crack-seal veins and viscous shear in subduction mélange. Geophysical Research Letters, 45, 5371–5379, https://doi.org/10.1029/2018GL078374

Vai, G.B. and Martini, I.P. 2001. Anatomy of an Orogen: the Apennines and the Adjacent Mediterranean Basins. Kluwer, Dordrecht.

Vannucchi, P., Remitti, F. and Bettelli, G. 2008. Geological record of fluid flow and seismogenesis along an erosive subducting plate boundary. Nature, 451, 699–703, https://doi.org/10.1038/nature06486

Vannucchi, P., Remitti, F., Bettelli, G., Boschi, C. and Dallai, L. 2010. Fluid history related to the early Eocene - middle Miocene convergent system of the Northern Apennines (Italy): Constraints from structural and isotopic studies. Journal of Geophysical Research, 115, 1–23, https://doi.org/10.1029/2009JB006590

Wang, K. and Hu, Y. 2006. Accretionary prism in subduction earthquake cycles: The theory of dynamic Coulomb wedge. Journal of Geophysical Research, 111, B06410, https://doi.org/10.1029/2005JB004094.

Wang, K., Brown, L., Hu, Y., Yoshida, K., He, J. and Sun, T. 2019. Stable forearc stressed by a weak megathrust: mechanical and geodynamic implications of stress changes caused by the M = 9 Tohoku-Oki earthquake. Journal of Geophysical Research, 124, 6179–6194. https://doi.org/10.1029/2018JB017043.

Watson, E.B. 2004. A conceptual model for near-surface kinetic controls on the trace-element and stable isotope composition of abiogenic calcite crystals. Geochimica et Cosmochimica Acta, 68, 1473–1488, https://doi.org/10.1016/j.gca.2003.10.003

Yamaguchi, A., Cox, S.F. and Kimura, G. 2011. Dynamic changes in fluid redox state associated with episodic fault rupture along a megasplay fault in a subduction zone. Earth and Planetary Science Letters, 302, 369–377, https://doi.org/10.1016/j.epsl.2010.12.029

Yamaguchi, A., Ujiie, K., Nakai, S. and Kimura, G. 2012. Sources and physicochemical characteristics of fluids along a subduction-zone megathrust: A geochemical approach using syn-tectonic mineral veins in the Mugi mélange, Shimanto accretionary complex. Geochemistry, Geophysics, Geosystems, 13, Q0AD24, https://doi.org/10.1029/2012GC004137